Nuclear quadrupole interaction due to point defects in aluminum: Effect of host lattice structure

M. J. Ponnambalam

Department of Physics, Bayero University, Kano, Nigeria

P. Jena

Department of Physics, Virginia Commonwealth University, Richmond, Virginia 23284

(Received 4 October 1984)

The electric field gradients (efg's) at the first four near-neighbor sites in Al caused by a vacancy, substitutional Mg, Si, Ga, Ge, In, and Sn impurities, and an interstitial positive muon have been calculated. The perturbed core as well as conduction-electron densities around the point defects are calculated self-consistently using the spherical solid model based on the density-functional theory. A critical discussion of the contributions to efg's from the bound and scattering electrons is given. The contributions to the efg's due to strain caused by the size difference between the host and impurity atoms are calculated by using an oscillatory form for the displacement field. Our theoretical results are in good agreement with available experimental data for all the alloys at all near-neighbor host sites.

I. INTRODUCTION

The electric field gradients (efg's) caused by impurities at near-neighbor host atom sites in cubic metals derive contributions from two main sources: the "valence effect" is due to the perturbation produced by the impurity on ambient electron distribution, and the "size effect" is due to the strain caused by the mismatch between host- and impurity-atom size. Although these two effects are intimately related to each other, for the sake of calculational convenience, they have been treated separately.

Kohn and Vosko[1] and Blandin and Friedel[2] showed that at large distances from the impurity, the valence-effect efg can be expressed in a simple form:

$$q^v(r) = \frac{8\pi}{3}\alpha(k_F)\delta n_a(r) \ , \tag{1}$$

where $\alpha(k_F)$ is the Bloch enhancement factor[1,3] due to the orthogonality of the conduction-electron states with host core orbitals. $\delta n_a(r)$ is the electron density at the asymptotic region and is given by the well-known Friedel formula.[1,2] Kohn and Vosko[1] were able to explain many qualitative features of efg's as a function of distance from the impurity, using the simple expression in Eq. (1). However, as new experimental data on efg's at first- and second-nearest neighbors became available,[4] it became apparent that the asymptotic formula is not valid at the first few near neighbors. Furthermore, the efg's in many alloy systems were found to deviate from cylindrical symmetry—contrary to the prediction from Eq. (1).

The next pioneering step in the development of the theory of efg was taken by Sagalyn and Alexander.[5] These authors used the preasymptotic expression for efg derived earlier by Jensen *et al.*[6] along with a new size-effect contribution to calculate the efg's at the first two near-neighbor sites in Cu alloys. Their prescription enables them to calculate the asymmetry in the efg tensor. With the help of two adjustable parameters [the Bloch enhancement factor $\alpha(k_F)$ and a coupling parameter λ for strain in size-effect efg], Sagalyn and Alexander[5] (SA) provided a satisfactory explanation of efg's in Cu-based alloys. The size-effect efg was calculated by drawing an analogy between the efg tensor and elastic tensor and by representing the displacement $u(\mathbf{r})$ of a host atom, a distance $\mathbf{r}$ from the impurity in elastic continuum theory as

$$u(\mathbf{r}) = D\mathbf{r}/r^3 \ . \tag{2}$$

The original prescription of SA, with minor modifications, is still used by many authors[6-8] to study efg's in cubic-metal alloys. Successful as they are, basic problems still remain in the SA procedure. For example, (1) the validity of the preasymptotic form of efg at the first few near neighbors is uncertain. (2) The method for evaluating the amplitudes and scattering phase shifts entering the expression for preasymptotic charge density adds further to the ambiguity. (3) Use of Eq. (2) to express the displacement of host ions implies that all host atoms around a given impurity must move in the same direction. This is known to be incorrect from both first-principles[9] and computer-simulation studies.[10]

The next major study in the theory of efg was carried out by the present authors.[11] We derived an exact expression for the valence-effect efg that is valid at all distances. The perturbed electron densities around the defect was calculated self-consistently by using the jellium model and the density-functional theory. For the strain contribution, we used an oscillatory form in contrast to that in Eq. (2). This theory was later applied by us[12] to study efg's in many Al-based alloys. We refer the reader to this paper which contains all the details of our methodology as well as an in-depth critique of earlier theories in this field.

This paper differs from our earlier calculations[12] in the following respects: (1) The perturbed electron densities around point defects are calculated in the spherical solid approximation[13] based on density-functional theory.[14] The spherical solid model goes beyond the jellium model where the host ions are smeared to form a homogeneous distribution of positive charges. Thus, the effect of a discrete host lattice on electron perturbation due to impurities is lost. In the spherical solid model, the host ions are replaced by pseudopotentials. The potentials of all atoms at a given distance from the impurity are then spherically averaged and added to the effective potential acting upon the electrons. This is a simple way to take into account the periodic nature of the host lattice. The use of this model in explaining the systematics of muon Knight shifts in many metallic hosts has been recently demonstrated by Manninen.[15] (2) We have also studied the relative contributions of bound impurity orbitals and scattering electrons to valence-effect efg. (3) A critical discussion of the use of an oscillatory form for the displacement field as opposed to Eq. (2) is also provided.

In Sec. II we outline only the essential steps of our theory needed to understand the efg results discussed in Sec. III. A summary of our conclusions and possible courses for future theories on efg are given in the concluding Sec. IV.

II. REVIEW OF THEORY

In a fcc metal, the principal axes of the valence-effect efg q^v and size-effect efg q^s tensors overlap. Thus, the total efg can be obtained by adding the corresponding principal components of q^v and q^s, namely,

$$q = q^v + q^s . \tag{3}$$

This, however, does not hold for the third-nearest-neighbor host atom. In this case it is necessary to add all six Cartesian components of q^v and q^s and then diagonalize the resultant to obtain the principal components of the tensor q. This can be achieved by using the α-function technique and rotation matrices.[7] However, if either q^v or q^s in Eq. (3) is vanishingly small for the third-nearest neighbor, the above procedure is not necessary. In the following we outline the salient features of the calculation of q^v and q^s.

A. Valence-effect efg, q^v

Assuming the induced electron density to be spherically symmetric around the impurity, we have shown[11,12] that the valence-effect efg can be given exactly by the equation,

$$q_{\parallel}^v(r) = \frac{8\pi}{3} \alpha(\mathbf{k}_F) \left[\delta n(r) + \frac{3}{4\pi r^3} [Z_{\text{eff}} - Z(r)] \right] , \tag{4}$$

where

$$\delta n(r) = n_I(r) - n_H(r) , \tag{5}$$

and

$$Z(r) = \int_0^r \delta n(r') d^3 r' . \tag{6}$$

$n_I(r)$ and $n_H(r)$ are the electron density distribution, respectively, around the impurity and host atom located separately at the origin. $Z_{\text{eff}} = Z(\infty)$ is the screening charge of the defect. q_{11} is referred to as the principal value of the efg. In situations where the efg does not possess cylindrical symmetry, another quantity η, the asymmetry parameter, is necessary to completely describe the efg tensor. By definition $0 < \eta < 1$. The location of the impurity atom in our calculation defines the origin of the coordinate system.

The electron density, n, around the host or impurity atom is composed of both core (bound) electrons n_b and conduction electrons n_{sc}. Thus,

$$n(r) = n_b(r) + n_{\text{sc}}(r) . \tag{7}$$

Similarly the number of electrons $Z(r)$ contained in a sphere of radius r around the origin consists of bound as well as scattering parts:

$$Z(r) = Z_b(r) + Z_{\text{sc}}(r) . \tag{8}$$

Thus, the valence-effect efg q^v in Eq. (4) derives contribution not only from the difference between the valence-electron structure of host and impurity atoms, but also from their differences in core configurations. Of course, the core electrons are much more localized than the valence electrons and may not affect efg's at host atoms far from the impurity. However, it is not so obvious that the core contributions at the first-nearest-neighbor site due to interstitial impurities or heavy substitutional impurities will be negligible.

To calculate $n(r)$ around the impurity or host atom in the spherical solid model, we express the external perturbation,

$$n_{\text{ext}}(r) = A\delta(\mathbf{r}) + n_0\Theta(\mathbf{r} - \mathbf{R}_{\text{WS}}) , \tag{9}$$

where A is the atomic number of impurity (host) atom and n_0 is the average valence-electron density of the host metal. $\mathbf{R}_{\text{WS}}$ is the Wigner-Seitz radius for the host. The corresponding electron density,

$$n(r) = \sum_{\substack{i \\ \text{occ}}} |\psi_i(r)|^2 , \tag{10}$$

is calculated by solving the Hohenberg-Kohn-Sham equation[14] (in Hartree a.u.):

$$\left[-\frac{\nabla^2}{2} + V_{\text{eff}} \right] \psi_i(r) = \epsilon_i \psi_i(r) . \tag{11}$$

ψ_i is the wave function of the ith occupied electron with eigenvalue ϵ_i. The effective potential V_{eff} is given by

$$V_{\text{eff}}(r) = V_{\text{es}}(r) + V_{\text{xc}}(r) + V_{\text{ss}}(r) . \tag{12}$$

The electrostatic potential V_{es} is obtained by using Eqs. (9) and (10) and solving the Poisson's equation. The exchange-correlation potential V_{xc} is obtained from the computed charge density by using the local-density approximation.[16] The spherical solid potential[13] V_{ss} is given by

$$V_{\mathrm{ss}}(r) = \frac{1}{4\pi} \int d\Omega \sum_{\nu}{}' \omega(|\mathbf{r} - \mathbf{R}_\nu|)$$

$$+ \int d^3 r' n_0 \frac{\Theta(r' - \mathbf{R}_{\mathrm{WS}})}{|\mathbf{r} - \mathbf{r}'|} , \tag{13}$$

where $\omega(|\mathbf{r} - \mathbf{R}_\nu|)$ is the bare-ion pseudopotential centered at the νth nucleus and the summation excludes the atom at the origin. For Al, we have used Aschroft's form[17] for $\omega(r)$ with the core radius of $1.12 a_0$. Equations (10)—(12) are solved self-consistently.

B. Size-effect efg, q^s

The components of the symmetric, traceless efg tensor q_{ij}^s, linear in the strain components ϵ_{ij}, are given by[5,12]

$$eq_{ij}^s = \delta_{ij}(F_{11} - F_{12})\left[\epsilon_{ii} - \frac{1}{3}\sum_k \epsilon_{kk}\right] + 2(1 - \delta_{ij})F_{44}\epsilon_{ij}, \tag{14}$$

where F_{ij}'s are components of a fourth-rank tensor. For a fcc host, these are given, in the point-ion model,[18] as

$$F_{11} - F_{12} = -3F_{44} = \frac{18\sqrt{2}\lambda e}{a_L^3} , \tag{15}$$

where a_L is the lattice constant and λ is the strain-coupling parameter needed to compensate for the fact that a solid is idealized by point charges. The elastic strain tensor is given in terms of the displacement field,

$$\epsilon_{ij} = \frac{1}{2}\left[\frac{\partial u_i}{\partial x_j} + \frac{\partial u_j}{\partial x_i}\right] . \tag{16}$$

Thus, the computation of $\hat{q}_{ij}^s$ requires a knowledge of the displacement $\mathbf{u}$.

We had earlier proposed for $\mathbf{u}$ an expression,

$$u(\mathbf{r}) = D\cos(2k_F r + \phi)\mathbf{r}/r^3 . \tag{17}$$

The choice of this form was *ad hoc*. It was proposed for the following main reasons: (1) It has an oscillatory form, thus enabling different host atoms to move either inward or outward depending on their distance from the impurity. As mentioned earlier in this paper, this is a desired feature which Eq. (2) lacks. (2) The simplicity of the form in Eq. (17) enabled us to carry out much of the strain-induced efg calculation analytically. (3) It has a form analogous to Friedel oscillations in screening electron density. (4) No other convenient form for $\mathbf{u}$ exists. Comparison of the efg results[12] using Eq. (17) with that using Eq. (2), clearly indicates that the former yields efg's in much better agreement with experiment.

The choice of $2k_F$ as a scaling factor, however, has no fundamental justification. This scaling factor perhaps should be more characteristic of the lattice than that of the electron. In this paper, we have therefore studied the dependence of our efg results on the choice of this factor. Therefore, we write

$$\mathbf{u}(\mathbf{r}) = D\cos(br + \phi)\mathbf{r}/r^3 . \tag{18}$$

It will be shown in the following section that a different choice of b in Eq. (18) only results in a different value for

λ, the strain-coupling parameter. The quality of the systematic agreement of calculated and experimental efg's and asymmetry parameters does not get affected. The phase factor ϕ is obtained from equilibrium conditions[19] and D is obtained by fitting the displacement of the first-nearest neighbor with either experimental or *ab initio* calculations based upon lattice statics. Again, we should point out that in the final expression for strain efg, it is the product λD that appears. Thus, the use of a precise value for D is not important in our calculation of efg systematics. It is for these reasons that we refer to our calculations as having only one adjustable parameter in practice.

To guide us in the choice of the scaling factor b in Eq. (21), we discuss a recent calculation of the lattice displacements and energies around a dipolar defect by Dick.[20] In an attempt to go beyond the continuum theory of elasticity, Dick[20] used the long-wave strain limiting form and a Debye model to study the defect-phonon interaction. He obtained analytic expressions for the displacement and strain field around the defect. In the asymptotic limit, the displacement has oscillatory terms, such as, $\cos(\tilde{g}_j - 3\pi/4)$ and $\cos(\tilde{g}_j - \pi/4)$, where

$$\tilde{g}_j = \begin{bmatrix} \tilde{g}_t \\ \tilde{g}_l \end{bmatrix}$$

$$= \left[\frac{48\pi}{1 + \frac{1}{2}(C_{44}/C_{11})^{3/2}}\right]^{1/3} \frac{r}{a_1}\left[\frac{1}{(C_{44}/C_{11})^{1/2}}\right] . \tag{19}$$

Here, a_1 is the first-nearest-neighbor distance and C_{44} and C_{11} are elastic constants. The suffixes t and l represent transverse and longitudinal mode, respectively. Substituting for C_{44}, C_{11}, and a_1 values[21] corresponding to Al, Eq. (19) gives, in a.u.,

$$\begin{bmatrix} \tilde{g}_t \\ \tilde{g}_l \end{bmatrix} = \begin{bmatrix} 0.962 \\ 0.507 \end{bmatrix} r . \tag{20}$$

For the scaling factor b in Eq. (18) we have used values $0.962 a_0^{-1}$ and $0.507 a_0^{-1}$. We should again caution the reader that the defects studied by Dick[20] are not the same as ours in this paper. The choices in Eq. (20) are only for guidance. The encouraging result is that the nature of agreement between calculated and experimental efg's are not sensitive upon this choice. Using Eqs. (18) in Eq. (14) we obtain for the νth-nearest neighbor,

$$q_{ij}^s = [\delta_{ij} - \tfrac{2}{3}(1 - \delta_{ij})]\left[\frac{18\sqrt{2}\lambda}{a_L^3}\frac{u_\nu}{r_\nu}\left[3 + \frac{b^2 r_\nu^2}{2}\right]\right]$$

$$\times \left[\frac{1}{3}\delta_{ij} - \frac{x_i x_j}{r_\nu^2}\right] . \tag{21}$$

Diagonalizing q_{ij}^s, the principal components of q^s are obtained. The net efg is given by
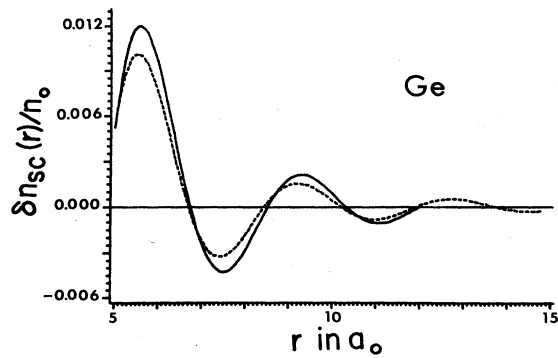
FIG. 1. Induced electron density distribution $\delta n_{sc}(r)$ [Eq. (5)] around substitutional Ge in Al, in the spherical solid model (dashed line) and pure jellium model (solid line).

$$q_{||} = q_{||}^{v} + q_{||}^{s} \; ,$$

$$q_{\perp}^{1} = q_{\perp}^{1v} + q_{\perp}^{1s} = -\tfrac{1}{2} q_{||}^{v} + q_{\perp}^{1s} \; ,$$ (22)

$$q_{\perp}^{2} = q_{\perp}^{2v} + q_{\perp}^{2s} = -\tfrac{1}{2} q_{||}^{v} + q_{\perp}^{2s} \; .$$

In this paper, we determine λ by fitting our calculated efg to experiment at the fourth-nearest neighbor around a monovacancy. Once λ is obtained, we keep it fixed for all impurities, i.e., we treat λ as a property of the host. In our earlier calculation, we varied λ from one impurity to another. In this regard, the present investigation also provides an improvement over our earlier calculations.[12]

III. RESULTS

A. Electronic structure

In Figs. 1 and 2 we plot the induced charge density around a Ge and Ga impurity atom in jellium (solid line) and spherical solid model (dashed line), respectively. The induced densities in these figures are shown relative to the ambient host densities. Note that in Ge, the spherical solid model result does not differ very much from the jellium result, whereas for Ga impurity, the two results differ substantially from each other up to the third-nearest-neighbor site. For other defects such as a vacancy, μ^{+}, Mg, Sn, and In, the differences between the spherical solid and jellium model results are similar to that of
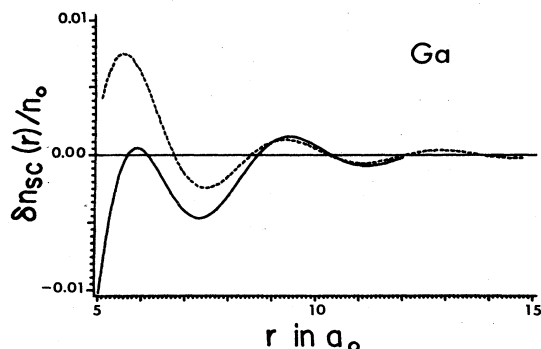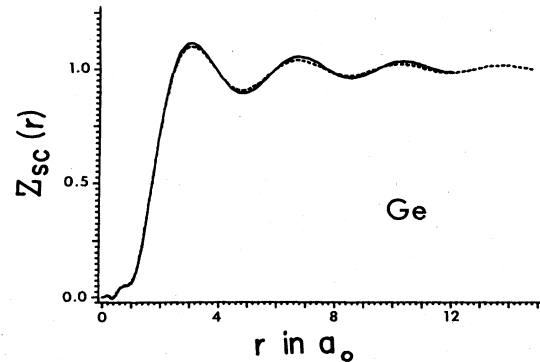

FIG. 3. Effective screening charge $Z_{sc}(r)$ [Eq. (6)] around substitutional Ge in Al, in the spherical solid model (dashed line) and pure jellium model (solid line).

Ge in Fig. 1.

In Figs. 3 and 4 we show the spatial dependence of the screening (scattering) charge, $Z_{sc}(r)$ for Ge- and Ga-impurity atoms in the spherical solid (dashed curve) and jellium (solid curve) model, respectively. Since the valence difference between Ge and Al is $+1$, $Z_{sc}(r)$ asymptotically approaches this value in Fig. 3. In Fig. 4, $Z_{sc}(r)$ asymptotically approaches zero since Ga and Al are isovalent. A comparison between Figs. 3 and 4 reveals that while Ge is screened at a shorter range, the screening radius for Ga is much larger. Thus, an isovalent impurity may provide a larger perturbation on the host electronic system than a heterovalent impurity. From Figs. 1–4, it is evident that the host lattice structure (modeled by a spherical solid approximation) may have significant influence on the valence efg through Eq. (4) in certain impurity cases such as Ga while in other situations, the jellium model may be adequate.

In Figs. 5 and 6, we plot the bound and scattering electron densities around Si- and Sn-impurity atoms, respectively, for distances relevant to the efg calculation. The electron densities from bound states are vanishingly small compared to the scattering electron densities for distances as small as first-nearest-neighbor distance. For interstitial impurities, since the nearest-neighbor distance decreases, the importance of the bound charges is expected to increase.

FIG. 2. $\delta n_{sc}(r)$ around Ga in Al. The rest of the legend is the same as in Fig. 1.
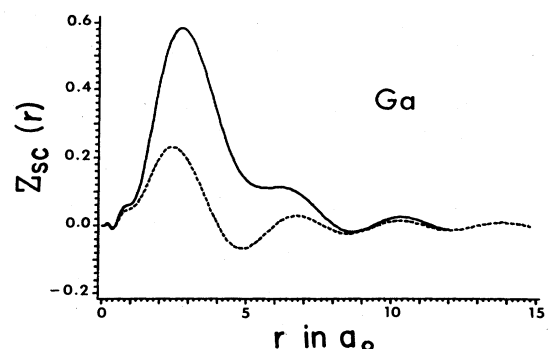

FIG. 4. $Z_{sc}(r)$ around Ga in Al. The rest of the legend is the same as in Fig. 3.
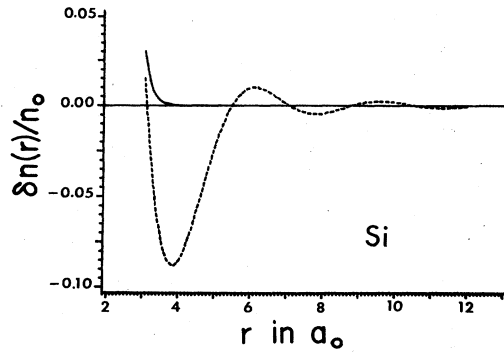
FIG. 5. Comparison of the bound charge $\delta n_b(r)$ (solid line) with the scattering charge $\delta n_{sc}(r)$ (dashed line) for the substitutional Si in Al. The bound part is magnified 100 times for clarity.

B. Valence- and size-effect efg

In Table I we compare the valence-effect efg at the first four near neighbors around vacancy, Mg, Si, Ga, Ge, Sn, and μ^+ defects. We note that in general the jellium model yields valence-effect efg's that are comparable to those obtained from the spherical solid model, except in a few exceptional cases.

In Table II we present the results of valence- and size-effect efg. To determine the size-effect contribution, we need to know the value of three parameters, D and b in Eq. (18) and λ in Eq. (21). Due to a lack of adequate information on the displacements of near-neighbor atoms around the point defects, we have used the changes in the lattice constant upon alloying $(1/a)da/dc$ as a guide to obtain the values of D in Eq. (18). The reader is referred to Ref. 12 for a detailed discussion of this procedure. We should again remind the reader that the results in Table II are not sensitive to the precise choice for D since the size-effect efg expression contains the term λD. And λ is, in our present calculation, an adjustable parameter. For the parameter b in Eq. (18), we have used the value of $0.962a_0^{-1}$. We obtain the strain-coupling parameter by fitting our calculated efg with experiment[4] at the first-near-neighbor site due to a vacancy. This yields a value of $\lambda = -6.7$. Keeping this value of λ, we have calculated the valence-, size-effect, total efg and asymmetry parameter at
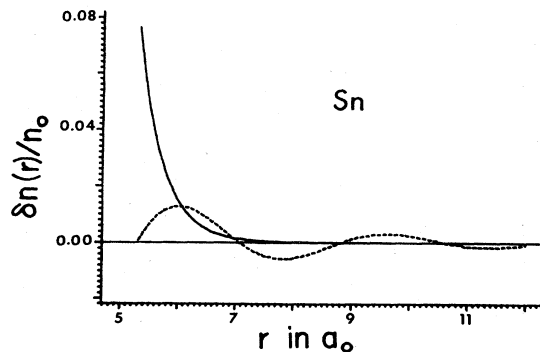

FIG. 6. Comparison of $\delta n_b(r)$ with $\delta n_{sc}(r)$ for Sn in Al. The rest of the legend is the same as in Fig. 5.

TABLE I. Comparison of $q_{\parallel}^v$ between the pure jellium model and the spherical solid model for impurities in aluminum. NN denotes nearest neighbor. The $\alpha(\mathbf{k}_F)$ values are taken from Ref. 3.

| | | $q_{\parallel}^v$ (Å^{-3}) | |
System	NN	Pure jellium	Spherical solid
Vacancy	1	−0.015	−0.005
	2	0.000	−0.004
	3	−0.004	−0.002
	4	−0.001	−0.002
Mg	1	−0.039	−0.040
	2	0.029	0.027
	3	−0.020	−0.019
	4	0.006	0.007
Si	1	0.095	0.077
	2	−0.030	−0.022
	3	0.024	0.015
	4	−0.009	−0.007
Ga	1	−0.089	0.090
	2	−0.048	−0.024
	3	0.018	0.015
	4	−0.008	−0.006
Ge	1	0.150	0.124
	2	−0.040	−0.030
	3	0.030	0.020
	4	−0.010	−0.009
In	1	0.126	0.114
	2	−0.031	−0.030
	3	0.020	0.019
	4	−0.006	−0.006
Sn	1	0.180	0.151
	2	−0.042	−0.035
	3	0.033	0.024
	4	−0.011	−0.010
μ^+ (octahedral interstitial)	1	0.273	0.162

the first four near-neighbor sites due to a vacancy, Mg, Si, Ga, Ge, In, and Sn impurities, and interstitial μ^+. The overall agreement between theoretical and experimental efg's is good. For the asymmetry parameter, however, the agreement can be best described as semiquantitative.

In order to examine the sensitivity of the computed efg's to the choice of the parameter b in Eq. (18), we have repeated the calculations presented in Table II by taking $b = 2k_F = 1.85a_0^{-1}$ and $b = 0.50a_0^{-1}$. The overall agreement between theoretical and experimental efg's remains satisfactory. As an example, we present in Table III a comparison of calculated efg's using three different values of b with experiment for the case of an Al-vacancy system. The corresponding values of λ obtained by fitting the first-nearest-neighbor efg are also given in Table III. Note that the values of λ increase significantly as the

TABLE II. Valence, size, and total efg in Å^{-3} for impurities in aluminum. Only the largest component of the efg tensor is shown in each case. $\lambda = -6.7$ for all.

System	$\dfrac{1}{a}\dfrac{da}{dc}$	NN	Theory q^v	q^s	$q = q^v + q^s$	η	Expt.[a] $\lvert q \rvert$	η
Vacancy	−0.100	1	0.003	−0.283	−0.280	0.36	0.280	0.65
		2	−0.004	−0.174	−0.178	0		0
		3	0.001	−0.079	−0.078	0.72	0.093	
		4	0.001	−0.063	−0.062	0.39	0.069	
Mg	0.099	1	0.020	0.216	0.236	0.05	0.195	0.07
		2	0.027	0.138	0.165	0		0
		3	−0.019	−0.056	−0.075	0.95	0.065	
		4	−0.003	0.050	0.047	0.57	0.033	
Si	−0.042	1	−0.038	−0.110	−0.148	0.52	0.282	0.03
		2	−0.022	−0.068	−0.090	0		0
		3	0.015	0.027	0.042	0.81	0.057	
		4	0.004	−0.025	−0.021	0.90	0.025	
Ga	0.045	1	−0.045	−0.070	−0.115	0.04	0.228	0.03
		2	−0.024	0.066	0.042	0		0
		3	−0.007	0.030	0.023	0.04	0.029	
		4	0.003	0.024	0.027	0.04		
Ge	0.045	1	−0.062	−0.070	−0.132	0.35	0.328	0.03
		2	−0.030	0.066	0.036	0	0.031	0
		3	−0.010	0.030	0.020	0.30	0.040	
		4	0.004	0.024	0.028	0.17	0.048	
In	0.060	1	−0.057	−0.091	−0.148	0.08	0.180	0.30
		2	−0.030	0.087	0.057	0	0.050	0
		3	−0.009	0.040	0.031	0.07	0.034	
		4	0.003	0.031	0.034	0.06	0.056	
Sn	0.39	1	−0.075	0.645	0.570	0.77	0.266	0.37
		2	−0.035	0.430	0.395	0	0.050	0
		3	−0.012	0.198	0.186	0.61		
		4	0.005	0.158	0.163	0.23	0.138	
μ^+ $f_1 = 0.025$[b] (octahedral interstitial)		1	0.162	0.395	0.557	0	0.18	0

[a]Experimental values are taken from Ref. 4.
[b]f_1 refers to the fractional displacement of the first NN. The first NN in Al-μ^+ is displaced outward by 2.5%.

values of b decrease. However, the overall agreement remains less sensitive, although showing steady sign of deterioration as the parameter b approaches zero.

IV. SUMMARY

In this paper we have presented the most exhaustive theoretical investigation of efg systematics to date due to several point defects in Al. The present study is an improvement over all earlier calculations[5-17] in several respects: (1) The valence-effect efg is calculated using an exact expression valid at all distances from the defect site. (2) The perturbation on the host conduction-electron distribution due to defects is treated self-consistently using the density-functional theory. The effect of impurity core states as well as the effect of host lattice structure on efg

are studied. (3) An oscillatory form for the displacement of host near neighbors is used to mimic observed features in lattice relaxation. A critical discussion for using this form to calculate size-effect efg and the dependence of

TABLE III. Comparison between efg's calculated for the Al-vacancy system and using three different values of the parameter b [see Eqs. (18) and (20)].

Nearest neighbor	Expt. $\lvert q \rvert$	Theory $b = 1.85$ $\lambda = -2.10$	$b = 0.96$ $\lambda = -6.70$	$b = 0.50$ $\lambda = -16.20$
1	0.280	−0.280	−0.280	−0.280
2		−0.187	−0.178	−0.161
3	0.093	−0.083	−0.078	−0.067
4	0.069	−0.067	−0.062	−0.052

efg's on various parameters entering the size-effect calculation is provided. (4) Only a single parameter λ is used to explain efg's at four near-neighbor sites due to eight different impurities. This has to be compared with published results[5-8] where the value of λ has varied by several factors in a given alloy system.

In spite of the above achievement, our theory does not match the same sophistication as that evident in experimental studies.[4] It is desirable to formulate a theory where (a) the size and valence effect can be unified, (b) the relaxation of the host near-neighbor positions and induced electron densities can be calculated self-consistently, (c) the perturbation of the host core electrons due to the presence of the electric field gradient can be incorporated in a self-consistent manner, and (d) all these effects can be utilized to calculate efg and asymmetry parameter η up to four near neighbors. Clearly, this poses a difficult challenge for the theorists, equipped with even the fastest

computer presently available. No formalism is known to these authors at present which can take into account the above features. Until such a procedure is available, we can draw comfort from the statement that from model calculations, it is possible to achieve a satisfactory understanding of efg systematics in cubic-metal alloys. We are presently trying to improve upon our theoretical model by incorporating the role of antishielding effects and eliminating the use of strain-coupling parameters by doing a direct lattice sum for the size-effect calculation.

ACKNOWLEDGMENTS

[1]W. Kohn and S. H. Vosko, Phys. Rev. 119, 912 (1960).
[2]A. Blandin and J. Friedel, J. Phys. Chem. Solids 17, 170 (1960).
[3]P. M. Holtham and P. Jena, J. Phys. F 5, 1649 (1975).
[4]G. Grüner and M. Minier, Adv. Phys. 26, 231 (1977); O. Hartmann, E. Karlsson, L. O. Norlin, D. Richter, and T. O. Niinikoski, Phys. Rev. Lett. 41, 1055 (1978); M. Minier, R. Andreani, and C. Minier, Phys. Rev. B 18, 102 (1978).
[5]P. L. Sagalyn and M. N. Alexander, Phys. Rev. B 15, 5581 (1977).
[6]B. L. Jensen, R. Nevald, and D. L. Williams, J. Phys. F 2, 169 (1972).
[7]K. K. Prasad Rao and N. C. Mohapatra, Phys. Rev. B 24, 1941 (1981); N. C. Mohapatra and S. Hafizuddin, Phys. Rev. B 27, 7776 (1983).
[8]S. D. Raj and S. Prakash, J. Phys. F 12, 1941 (1982); B. Pal, S. D. Raj, and S. Prakash, Can. J. Phys. 61, 1064 (1983); S. D. Raj, J. Singh, and S. Prakash, Phys. Rev. B 27, 2241 (1983).
[9]S. P. Singhal, Phys. Rev. B 8, 3641 (1973); F. Perrot and M. Rasolt, Solid State Commun. 36, 579 (1980); G. Solt, M. Manninen, and H. Beck, J. Phys. F 13, 1379 (1983); M. J. Puska and R. M. Nieminen, Phys. Rev. B 29, 5382 (1982).
[10]L. A. Girifalco and V. G. Weizer, J. Phys. Chem. Solids 12, 260 (1960).
[11]M. J. Ponnambalam and P. Jena, Phys. Rev. Lett. 46, 610 (1981).
[12]M. J. Ponnambalam and P. Jena, Hyperfine Interact. 20, 65 (1984).
[13]C. O. Almbladh and U. von Barth, Phys. Rev. B 13, 3307 (1976).
[14]P. Hohenberg and W. Kohn, Phys. Rev. 136, B864 (1964); W. Kohn and L. J. Sham, Phys. Rev. 140, A1133 (1965).
[15]M. Manninen, Phys. Rev. B 27, 53 (1983).
[16]O. Gunnarsson, B. I. Lundqvist, and J. W. Wilkins, Phys. Rev. B 10, 1319 (1974).
[17]M. Manninen and R. M. Nieminen, J. Phys. F 9, 1333 (1979).
[18]E. A. Faulkner, Philos. Mag. 5, 843 (1960).
[19]S. P. Timoshenko and J. N. Goodier, Theory of Elasticity (McGraw-Hill, New York, 1970).
[20]B. G. Dick, Phys. Rev. B 24, 2127 (1981).
[21]G. A. Kamm and G. A. Alers, J. Appl. Phys. 35, 237 (1964).